

HANDI: Hand-Centric Text-and-Image Conditioned Video Generation

Yayuan Li^{1,*} Zhi Cao^{1,*} Jason J. Corso^{1,2}
¹University of Michigan ²Voxel51
[Project Page](#)

Abstract

Despite the recent strides in video generation, state-of-the-art methods still struggle with elements of visual detail. One particularly challenging case is the class of videos in which the intricate motion of the hand coupled with a mostly stable and otherwise distracting environment is necessary to convey the execution of some complex action and its effects. To address these challenges, we introduce a new method for video generation that focuses on hand-centric actions. Our diffusion-based method incorporates two distinct innovations. First, we propose an automatic method to generate the motion area—the region in the video in which the detailed activities occur—guided by both the visual context and the action text prompt, rather than assuming this region can be provided manually as is now commonplace. Second, we introduce a critical Hand Refinement Loss to guide the diffusion model to focus on smooth and consistent hand poses. We evaluate our method on challenging augmented datasets based on EpicKitchens and Ego4D, demonstrating significant improvements over state-of-the-art methods in terms of action clarity, especially of the hand motion in the target region, across diverse environments and actions.

1. Introduction

Videos have become commonplace to learn the intricacies of new skills or refresh forgotten ones, such as cooking a certain dish or fixing a broken bicycle [3, 4, 9, 11, 43, 80–82, 88, 98], including significantly complex skills like surgery [18]. Learning from videos is so central to modern society that more than fifty percent of YouTube viewers seek instructional content [76]. One particularly important class of videos are ones that demonstrate sequences of goal-oriented actions usually involving dextrous hand motion and interaction with tools, objects, and the environment [26, 32, 89, 112]. This class of videos has even demonstrated extensive effectiveness in robot learn-

ing [5, 17, 23, 30, 42, 45, 60, 68, 100, 100, 101, 110].

The vision community has generated numerous relevant video benchmarks, like Assembly101 [74], YouCook2 [112], Meccano [70], and HoloAssist [87]. However, these benchmark videos are rarely available in arbitrary working environments where humans or robots operate. Although humans possess varying abilities to learn under environment variation and distraction [24], such factors pose significant challenges for robots or other AI agents, limiting the applicability to broader scenarios [79]. Recent work has explored the generation of instructional images [47, 79] or the retrieval of existing videos for reference [4, 33], with limited success. But, images do not highlight the temporal flow of actions, requiring challenging extrapolation, and the retrieved videos have various distractions, such as a different visual appearance of target objects, different view points, and background variations, which increase cognitive load for human learners [16] and is actually harmful to robot policy learning [17, 42, 60].

To address this gap, we consider a new problem that seeks to generate such goal-oriented hand-centric videos. We refer to this problem as hand-centric video generation or HCVG. Ideally, the generated videos would be usable for such human or robot skill learning, or they may be generally useful as in the broader case of video generation. Concretely, HCVG assumes text and image input, similar to image generation work [47, 79]. The text describes the target instructional action and the RGB image provides the context of the visual environment. As shown in Fig. 1, the generated hand-centric videos are expected to showcase the consistent motion of the target action with a clear subject (the hand and any tools and objects in use) appearance.

The intricacies of this complex hand-centric motion are easily observed in any of the popular instructional video datasets, like HowTo100M [62], Recipe1M [61], and YouCook2 [112]. At the same time, the generated videos should not introduce any unnecessary distractions: e.g., after “cutting a carrot,” the carrot should actually be rendered as a bunch of carrot pieces, but the rest of the environment should not be changed (no hallucinations in the background, no lighting changes, no camera movements, and so on).

*Equal contribution

¹Video results can be found on the [Project Page](#)

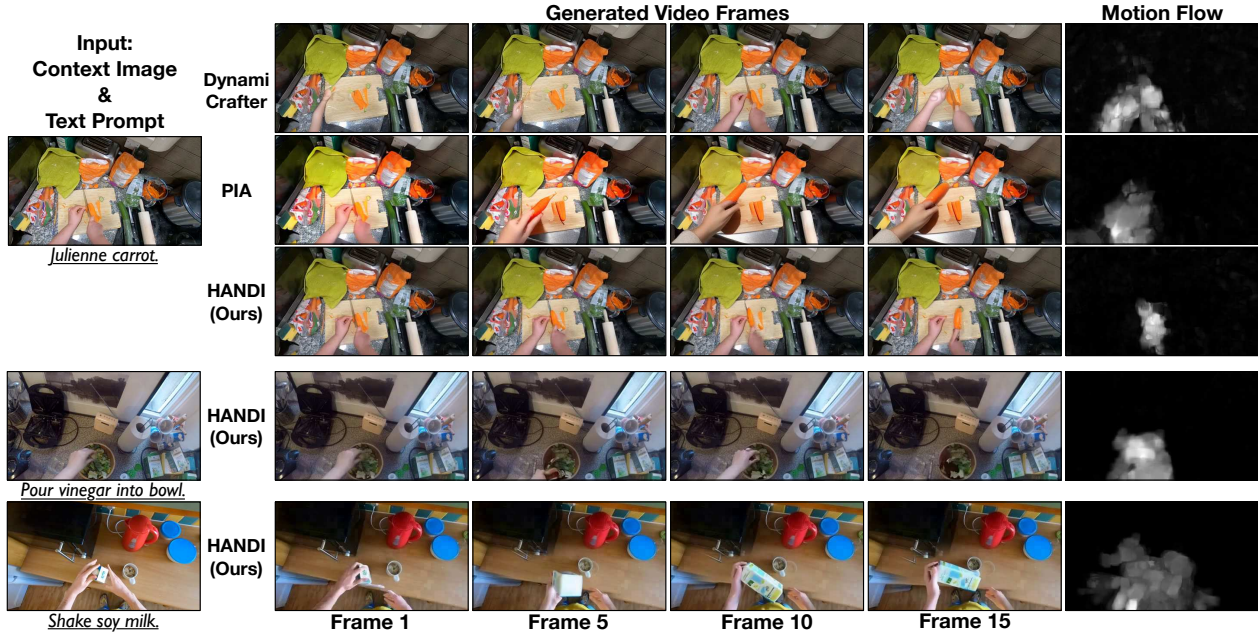


Figure 1. Illustration of our proposed Hand-Centric Text-and-Image Conditioned Video Generation (HCVG). Given an image for context and an action text prompt, our method generates video frames with precisely refined hand appearance and motion, overcoming challenges like unreasonable motion in backgrounds. Unlike baselines that extend unnecessary motion to background with rough hand structure, our approach produces motion in more reasonable area, as shown in the Motion flow visualization and refined hand details.

Importantly, the new HCVG problem is different than the instruction-based editing problem in works like InstructPix2Pix for images [12], 3D [35, 95], and video [15, 31, 106]. Although many of these works use an image-conditioned diffusion model, the tasks and necessary modeling are distinct. In hand-centric video generation, given an image and a text prompt, the task is to generate a video given the desiderata described above. Likewise, HCVG is different than the numerous text-to-video works [40, 53, 59, 91, 107], as these works do not support an image as input context with the text prompt, and such an extension is non-trivial.

On the other hand, HCVG is closely related to the well-known text-and-image to video (TI2V) problem. TI2V methods, such as TI2V-Zero [66] and PIA [109], extend text-to-image (T2I) models [71, 72] to produce videos conditioned on images and text. However, there are critical differences between them that, despite the advances in TI2V, make HCVG a distinct challenge. As we detail below, these include the ability to avoid distracting content and to generate high-quality hand motions with realistic appearance including object effects from the actions.

First, existing TI2V work focuses on content that is scenery-, character- or object-centric. In those videos, the motion area (MA)—the spatial region in the input image (and generated video) in which to focus the generation of target actions; MA is a term we adopt from AnimateAnything [25]—dominates because of the large target size and

the typically clean background (for character- and object-centric cases). In contrast, the hand-centric videos in study usually have fine-grained motion with a small subject (e.g., hand) carrying out a well-defined task, surrounded by arbitrary, sometimes quite cluttered backgrounds. Unfortunately, as shown in Fig. 1 contemporary TI2V methods lead to distracting content like a hallucination in the background (e.g., a hand pops up).

Even though some work has identified these challenges in hard samples, they rely on the extra user input of the MA [25] or even motion trajectory [52, 105], which does not scale. Moreover, the MA is a function of the specific activity and may vary throughout the generated video; hence in HCVG it must be automatically computed. Recent works about robotic policy learning via video generation [27, 78, 101] mitigate the hallucination issue by fitting a huge amount of training samples, but they still struggle with camera movement in the generated videos because the training videos contain significant amounts of it, which is known to be highly distracting for learners [13, 44].

Second, generating high-quality articulated hand motion is important but hard. The generated hand must be consistent—smooth and non-flickering hand pose in consecutive frames. And, yet, consistent is not enough: it must also capture the semantics of the task described by the prompt, showcasing the correct motion and interaction with the environment, tools, and objects within it, as depicted in the input image and necessitated by the text

prompt. Existing visual generation techniques, such as VideoCrafter [20, 21] and DragNUWA [105] among many, e.g., [57, 64, 67, 102], focus on general-purpose synthesis but are less effective in meeting these critical HCVG needs.

To overcome these technical challenges, we propose a novel hand-centric video generation method—we call it HANDI for hand-centric diffusion—that automatically infers the MA and incorporates a Hand Refinement Loss with a 3D diffusion model (space-time) as the backbone [39, 71]. HANDI has a two-stage approach for HCVG, both stages are diffusion-based in 3D space-time. In the first stage, we learn a model to infer the MA from the input image and text prompt. In the second stage, we augment the diffusion backbone with an innovative Hand Refinement Loss, since the consistency of motion and appearance of the hand is critical in HCVG. Importantly, we incorporate the learned motion area mask so that the stage 2 diffusion model can implicitly learn about object state changes that occur when the hand is carrying out the action specified in the prompt, without a need to explicitly model the object state.

We augment two previous action-oriented image generation datasets [47] based on Ego4D [32] and EpicKitchens [26] for evaluation. In addition to various standard video generation metrics, we propose two additional metrics focusing on good MA and hand appearance. We first compare with SOTA video generation methods to show HANDI’s effectiveness, demonstrating our method’s strong performance for HCVG. Then, we take a closer look at model performance along key axes: (1) the performance of samples with large MA and motion complexity defined by hand movement, (2) the ability to capture the fine-grained motion of the hands, (3) the performance within the MA versus the whole frame, and (4) compute time needed given the two-stage nature of our method. We show that our model outperforms SOTA baselines along each of these axes. Our key contributions are two-fold:

1. We identify the unique aspects of hand-centric video generation (HCVG) and propose a new method, HANDI, that is able to address these unique challenges.
2. We demonstrate that HANDI is able to outperform state of the art video generation from image and text-prompt methods, along all measurement axes.

All code, data, and benchmarks will be open-sourced, including the ability to reproduce every included result.

2. Hand-Centric Video Generation

Problem Statement Formally, we define the hand-centric text-and-image conditioned video generation (HCVG) problem as follows. Given an RGB image $I \in \mathbb{R}^{H \times W \times 3}$ containing a manipulator (a hand or hands) ready to perform an action, and a text prompt T to describe the action, an HCVG method will output an RGB video clip

$V \in \mathbb{R}^{L \times H \times W \times 3}$ demonstrating how the action in T is done in the same visual environment shown in I . We reserve notation I for specifying this *visual context*. In the remainder of the paper, we adopt a shorthand notation when specifying the dimensions of matrices: let $\boxtimes \doteq H \times W$ and it subsumes neighboring \times . So, $I \in \mathbb{R}^{\boxtimes 3}$ and $V \in \mathbb{R}^{L \boxtimes 3}$.

Training Data Expectations Given the rich instructional and action-oriented video corpora [26, 32, 61, 62, 70, 74, 87, 112], we can assume a corpus of training videos for HCVG. Each training sample will be comprised of a training video $V \in \mathbb{R}^{(L+1) \boxtimes 3}$ and a text prompt T describing the goal-oriented activity in the video. The first frame of V serves as the visual context I for HCVG. The remaining L frames are the ideal video generation output given I and T .

Method Overview

We adapt SOTA video latent diffusion techniques [28, 65, 90] to be the core of our solution to the HCVG problem. Our model has two stages: stage 1 generates the motion area mask and stage 2 generates the video. However, we use the same diffusion backbone for both stages, simplifying our discussion.

Action Text Embedding Let us first explain how we represent that action text prompt T to allow us to effectively condition the generation process on it. To generate the *action text embedding*, E_{text} , we first expand T using a pre-trained instruction tuning module [47] to generate a rich textual description based on the evidence that this improves conditional diffusion models [14, 47, 79, 108]. After expansion, we use the CLIP text embedding [69] to compute $E_{text} \in \mathbb{R}^{N \times d}$ where N is the number of tokens and d is the feature dimension.

Training Consider a training video $V \in \mathbb{R}^{(L+1) \boxtimes 3}$ and its associated action text embedding E_{text} . We process V frame-by-frame with the pre-trained VAE encoder from Stable Diffusion v1.5 [71] to compute the latent video, which is common practice [25, 28, 39, 75, 90]. After concatenating the prior or generated motion area mask (described in §2.1), we arrive at $z \in \mathbb{R}^{(L+1) \boxtimes (c+1)}$, where c is the latent space dimensionality. We remove the extra one timestamp to produce the L -frame target video.

For each diffusion training forward step, following standard practices [55, 56, 71], we prepare the noisy latent video z_t for a randomly sampled $t \in 1, \dots, \tau$ where τ is a pre-defined max step, according to standard noise-adding process [38, 67]:

$$z_t = \sqrt{\prod_{i=1}^t (1 - \beta_i)} z_0 + \sqrt{1 - \prod_{i=1}^t (1 - \beta_i)} \epsilon, \quad (1)$$

where β_i is a predefined coefficient that controls noise intensity at step i and $\epsilon \sim \mathcal{N}(0, \mathbf{I})$ is the sampled Gaussian noise. Then, we use a 3D UNet-based Noise Predictor [25], aligned with recent video generation work [28, 39, 71, 75,

90], to predict the noise $\hat{\epsilon}_t$ during the denoising process. The noise predictor takes the current noisy latent sample z_t and conditions on the E_{text} for prediction. Each of its blocks contains convolution layers [49] for spatial information extraction at the per frame level, temporal convolution layers [48, 84] and temporal attention layers [99] for information fusion across all timestamps at video level, and extra cross attention layers [85] to fuse information from E_{text} .

Inference Starting with visual context I , we produce $z_{context}$ from the pre-trained VAE encoder (also by Stable Diffusion v1.5 [71]). Following [25], we duplicate $z_{context}$ for L times and concatenate the prior or generated MA mask, depending on stage (§2.1). Then we apply Eq. (1) at the max noise step τ to produce the initial noisy latent video z'_τ as the beginning of denoising process. The denoising process during inference iterates τ steps. At each denoising step t the trained stage-specific noise predictor model conditionally predicts the noise $\hat{\epsilon}_t$ from z'_t , the same as training process. We apply the DPM++ solver [55, 56] to calculate the noisy latent video at previous timestamp z'_{t-1} iteratively for τ times. After τ steps of denoising, a clean latent video z'_0 is produced. The pretrained VAE decoder [71] is applied per-frame to produce the generated motion area mask video or generated video in pixel space. We follow Dai et al. [25] to explicitly enforce the mask after the generation process, replacing the background pixels from the context image I .

Innovations Extending this structure, we introduce two main innovations. First (§2.1), we develop a spatially cued approach that automatically learns the motion area mask given visual context I and text prompt T . This is critical for HCVG as the video generation needs to focus in on the pertinent area of the video while leaving the rest of it undisturbed to avoid distraction. Furthermore, it encourages the implicit learning of object state changes that frequently occur in our class of videos. Second (§2.2), we propose a novel Hand Refinement Loss tailored to HCVG. This loss greatly helps the generated video deliver higher quality critical details of action information since the hand is the key element when demonstrating actions in this scenario. We describe these two innovations in more detail next, followed by their integration into the full loss in Sec. 2.3.

2.1. Automatically Estimating the Motion Area

Hand-centric video generation must focus its effort on the spatiotemporal region that will contain the actual hand-object interaction, to avoid manipulating the visual context and adding distraction in the background. Hence, a spatiotemporal mask is needed. Although past work has supported the use of a human-supplied spatial mask in video generation [25], we focus on automatically generating the mask because it is less onerous and more flexible. The first stage of our conditional diffusion model must produce a mask video that includes any and all parts of the video that

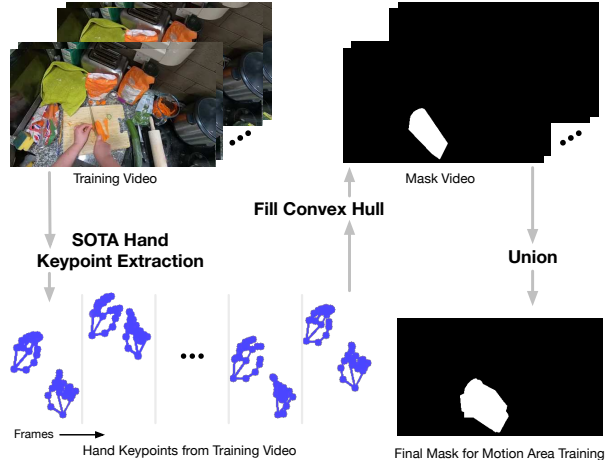


Figure 2. Training motion area masks are automatically created from the training videos. We flood fill the convex hulls of the hand regions, and then take the set-union of these over all frames.

may be used in the execution of the actor given visual context I and action text prompt T , which are used during the diffusion process.

For the MA generation, we assume that the relevant regions of activity map to the extent of the hands in the training videos. We hence automatically annotate the motion area in a training video using off-the-shelf SOTA hand keypoint detection [58], as shown in Fig. 2.

Concretely, given a training video $V \in \mathbb{R}^{(L+1) \times 3}$ (including the context image as the first frame), we apply the SOTA hand keypoint detector, denoted as Υ , that outputs, for each frame $l = [0, 1, 2, \dots, L]$, a set of hand keypoints $P_l \in \mathbb{R}^{J_l \times 2}$ where J_l is the number of 2D keypoints detected for frame l . For each P_l , we floodfill their convex hull to delimit a region as the mask M_l at frame l . We then apply union over masks for all frames to produce the final MA mask $M_{video} \in [0, 1]^{\square}$ for training.

During training of the stage 1 noise predictors, these mask videos are used as the targets. Since we use the same diffusion model structure for both stages, we also supply a prior mask during stage 1 training. This prior mask is computed as the normalized coverage over all groundtruth masks in the training set, indicating the prior distribution of the MA. During stage 2, the soft region masks outputted from stage 1, post-processed with morphology, are incorporated as part of the conditioning for the video generation. Our experiments show the high impact of the MA (§Sec. 3).

2.2. Hand Refinement Loss

It is critical yet challenging to show detailed hand appearance with consistency in action-specific motion in hand-centric video generation: the hands are typically relatively small in the pixel-space, the hands are articulated, the motion is intricate, and the background is often cluttered. We hence propose a new Hand Refinement Loss (HRL) func-

tion \mathcal{L}_{HR} that improves the subtle but critical details, emphasizing the hands (see Fig. 3). Our approach is more lightweight (applied as a loss function) than previous hand generation work which require a separate model or heavy post processing [29, 57, 64, 102].

Let us define the representation of the hand. In a given frame l , let $P_l \in \mathbb{R}^{j \times 2}$ ($j \in \{0, \dots, J\}$) represent the hand structure, containing the 2D coordinates of the J joints. In this work, we assume there are at most two hands in one frame, aligned with popular hand-centric activity datasets (e.g., EpicKitchens and Ego4D [26, 32]). We follow a commonly used hand pose skeleton topology [58] which defines 21 joints to represent structure of one hand. Therefore, J is set to 42 in all our experiments.

We compute the Hand Refinement Loss between the generated video $V^{\text{gen}} \in \mathbb{R}^{L \times 3}$ from stage 2 and the input training video $V^{\text{train}} \in \mathbb{R}^{L \times 3}$, both not including the input context image. To produce P_l^{gen} and P_l^{train} , we first apply the SOTA hand pose detector Υ on both videos [58]. Υ is aware of the temporal information in the video and configured to produce joint coordinates for left and right hands. We normalize the joints detected by Υ in terms of frame size to $[0, 1]$. If some joints in the skeleton topology are not detected by Υ (i.e., the number of detected joints is less than J), we set the coordinates of the missing joints in either P_l as 0. Those missing joints hence do not contribute to model optimization for this frame, but the same computational efficiency is maintained.

The point of adding the hand refinement loss is to encourage the generation of realistic, articulated hand pose for the specified activity. We hence freeze the hand detector Υ and optimize the stage 2 noise predictor to encourage better hand rendering, as follows. Given the hand pose sequences in the training and generated videos, we compute the Mean Square Error (MSE) between them as the loss value:

$$\mathcal{L}_{HR} = \frac{1}{L} \sum_{l=1}^L \frac{1}{J} \|P_l^{\text{gen}} - P_l^{\text{train}}\|_F^2. \quad (2)$$

Note that \mathcal{L}_{HR} starts to contribute densely at the latter iterations of the training when the rough hand structure in the generated video can be detected by Υ . Clearly, computing \mathcal{L}_{HR} requires the decoded video V^{gen} available; we compute this video at each training iteration directly from the denoised latent video z'_0 (see §2.3, Eq. (4)).

2.3. Latent- and Pixel-Space Loss Portfolio

With our innovations in automatically generating the MA mask and in the hand refinement, we require loss computation both in the latent and the pixel space at each stage.

Latent Space We define our the noise prediction loss \mathcal{L}_{noise} as follows, reflecting the conditions from input

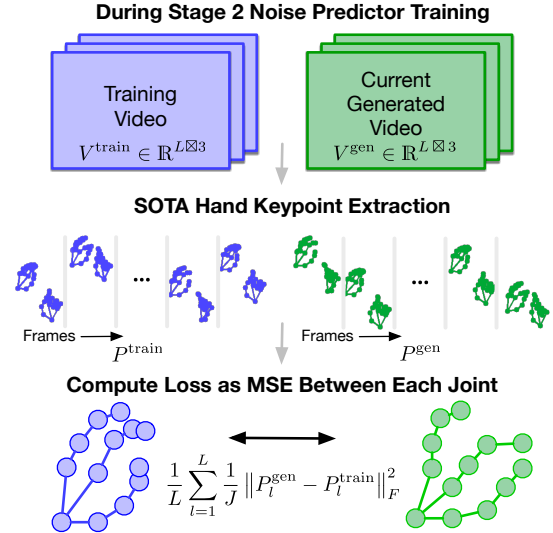


Figure 3. Illustrates the Hand Refinement Loss that drives the stage 2 noise predictor to focus on the fine-grained detailed of the hand pose in the context of the interaction. Bottom pose is for illustration only. Our representation has 21 joints per hand.

video, text, and MA mask for HCVG:

$$\mathcal{L}_{noise} = \mathbb{E}_{(V, E_{text}, M_{\{prior, gen\}}), \epsilon \sim \mathcal{N}(0,1), t} [\|\epsilon - \epsilon_{\theta}(z_t, t)\|_2^2] \quad (3)$$

where V is the training video (including the context image I), E_{text} is the feature representation of action prompt, $M_{\{prior, gen\}}$ is the prior or generated MA mask for stage 1 or 2 respectively, ϵ is the sampled Gaussian noise and ϵ_{θ} is the noise predicted by the noise predictor $D_{\{1,2\}}$ conditioned on the noise-added latent video z_t with the randomly sampled noise step t .

Pixel Space For the pixel-level loss \mathcal{L}_{mIoU} and \mathcal{L}_{HR} , we first decode the denoised latent video z'_0 to the pixel space and then compute the loss between the generated video and the target video. We obtain the clean latent video z'_0 by the following equation:

$$z'_0 = \frac{z_t - \sqrt{1 - \prod_{i=1}^t (1 - \beta_i)} \epsilon}{\sqrt{\prod_{i=1}^t (1 - \beta_i)}}. \quad (4)$$

Then, we decode the actual video V^{gen} from z'_0 , using the same process we described above during inference.

Stage 1 Loss We apply a mIoU loss \mathcal{L}_{mIoU} in pixel space in addition to \mathcal{L}_{noise} to have the final loss:

$$\mathcal{L}_{stage1} = \mathcal{L}_{noise} + \alpha \mathcal{L}_{mIoU} \quad (5)$$

where α is a hyperparameter tuned empirically. The Mean Intersection over Union (mIoU) loss is defined as

$$\mathcal{L}_{mIoU} = 1 - \frac{1}{L} \sum_{l=1}^L \frac{\sum_{i,j} (M_i^{\text{gen}} \cdot M_j^{\text{train}})}{\sum_{i,j} (M_i^{\text{gen}} + M_j^{\text{train}} - M_i^{\text{gen}} \cdot M_j^{\text{train}})}, \quad (6)$$

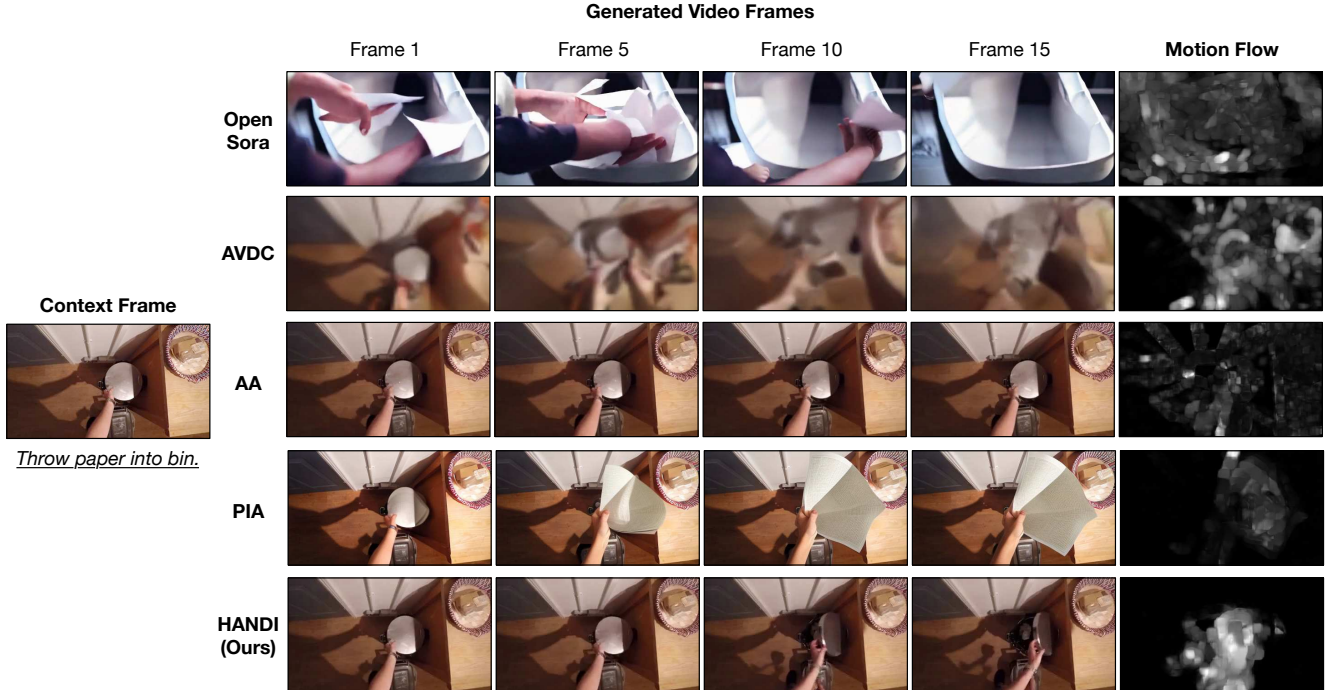


Figure 4. Qualitative results comparing with baselines. Our method generates videos that contain subtle hand motion that corresponds to the action description. This is because our method focuses on the effective motion region instead of cluttered background and our method is optimized with a tailored Hand Refinement Loss. The motion flow of the generated video provides more straightforward visualization and yield the same conclusion. Please see more video results in supplementary materials.

where M_l^{gen} and M_l^{train} are the generated and training binary masks for frame l , summed over spatial dimensions i and j . L denotes the number frames in the output video.

Stage 2 Loss We apply the Hand Refinement Loss \mathcal{L}_{HR} in addition to \mathcal{L}_{noise} to have the final loss:

$$\mathcal{L}_{stage2} = \mathcal{L}_{noise} + \eta \mathcal{L}_{HR} \quad , \quad (7)$$

where the coefficient η is a hyperparameter.

3. Experiments

Datasets Existing video generation benchmarks mostly feature aesthetically filtered or professionally edited web videos, covering diverse topics [2, 7, 8, 10, 22, 41, 50, 72, 73, 86, 96]. We instead evaluate our method on two widely used hand-centric interaction video benchmarks: Epic-Kitchens-100 (EK) [26] and Ego4D [32], using the quality-checked versions released by LEGO [47]. EK contains 60429/8857 train/test samples and Ego4D contains 85521/9931 train/test samples. The average video length are 2.4/1.07 seconds for EK/Ego4D. We choose EK and Ego4D as they are raw and unfiltered recordings focusing on hand actions, manually captured by research teams. As a result, they reflect real-world challenges such as cluttered backgrounds, weak lighting conditions, and natural scene variations while maintaining diversity in actions (97/1772 unique verbs in EK/Ego4D), objects

(300/4336 unique nouns in EK/Ego4d), and environments (45/74 kitchens/locations in EK/Ego4D).

Method	Parameters	Inf. Time (s)
LFDM [65]	0.108	3.57
AA [25]	1.837	5.74
AVDC [104]	0.229	66.23
PIA [109]	1.483	13.8
Open Sora [111]	1.484	44
DynamiCrafter [93]	1.876	9.32
CogVideoX [103]	4.978	108.41
HANDI	3.674	8.64

Table 1. Efficiency results for the HANDI method on EpicKitchens benchmark. The table lists various parameters and their corresponding efficiency values.

Metrics We conduct a comprehensive quantitative evaluation. For *visual similarity* between generated and ground truth videos, we use the image-to-image Fréchet Inception Distance (FID) [37] and CLIP_{GT} score [69] as our averaged frame-level similarity, and the Fréchet Video Distance (FVD) [83] and EgoVLP score [47, 54] at the video level. For *semantic similarity* between the prompt and the generated video, we adopt the frame-level CLIP_{Tx} score [92] and the video level BLIP score [47, 51]. We measure *motion coherency* of the generated video. We apply the Consistency CLIP score CLIP_{Cs.}, an average CLIP similarity between consecutive frames [69]. FVD also reflects tempo-

Benchmark	Method	HS-Err. ↓	VisualSim.-Frame		VisualSim.-Video		Consistency	SemanticSim.	
			FID ↓	CLIP _{GT} ↑	FVD ↓	EgoVLP ↑		CLIP _{Cs.} ↑	CLIP _{Tx.} ↑
EpicKitchens	LFDM [65]	0.01987	39.37	0.9241	129.80	0.354	0.9826	28.37	0.235
	AA [25]	0.01908	<u>5.49</u>	<u>0.9588</u>	171.29	0.338	0.9843	29.97	<u>0.295</u>
	AVDC [104]	0.01969	140.34	0.8918	81.39	0.197	0.9582	24.66	0.116
	PIA [109]	0.01826	24.70	0.9446	212.88	<u>0.361</u>	<u>0.9849</u>	<u>30.06</u>	0.294
	Open Sora [111]	0.01968	135.34	93.823	124.52	0.187	0.9573	24.46	0.186
	DynamiCrafter [93]	<u>0.01716</u>	43.56	0.9306	175.79	0.348	0.9131	28.22	0.288
	CogVideoX [103]	0.01981	127.51	0.9362	121.06	0.214	0.9677	25.13	0.176
HANDI	0.01512	5.27	0.9590	<u>101.89</u>	0.377	0.9896	31.14	0.298	
Ego4D	LFDM [65]	0.02127	50.67	0.9204	126.71	0.535	0.9821	26.93	0.221
	AA [25]	0.02393	<u>21.83</u>	<u>0.9647</u>	129.60	<u>0.642</u>	<u>0.9894</u>	28.56	<u>0.260</u>
	AVDC [104]	<u>0.02117</u>	144.91	0.8816	107.82	0.261	0.9722	24.17	0.155
	PIA [109]	0.02393	34.62	0.9457	<u>104.38</u>	0.603	0.9746	29.15	0.219
	Open Sora [111]	0.02142	141.90	0.8716	117.87	0.252	0.9753	24.12	0.172
	DynamiCrafter [93]	0.02203	57.21	0.9386	181.24	0.336	0.9489	26.67	0.231
	CogVideoX [103]	0.03079	187.20	0.8962	165.18	0.201	0.9900	28.22	0.147
HANDI	0.01939	21.51	0.9651	103.15	0.664	0.9873	<u>28.63</u>	0.263	
Motion Intensive	LFDM [65]	0.02053	56.95	0.9254	137.44	0.303	0.9825	28.39	0.210
	AA [25]	<u>0.01764</u>	<u>23.93</u>	0.9591	115.14	<u>0.368</u>	<u>0.9845</u>	30.07	0.276
	AVDC [104]	0.02143	148.11	0.8933	85.97	0.204	0.9579	24.60	0.102
	PIA [109]	0.01940	40.97	0.9448	217.59	0.330	0.9719	<u>30.09</u>	<u>0.280</u>
	HANDI	0.01663	23.79	<u>0.9589</u>	<u>114.52</u>	0.371	0.9849	31.12	0.327

Table 2. Quantitative results on EpicKitchens [26], Ego4D [32] and a Motion Intensive subset of EpicKitchens. HANDI (ours) outperforms all baselines across all metrics on at least one benchmark. VisualSim.-Frame represents the aspect of visual similarity at frame level; VisualSim.-Video represents visual similarity at video level; SemanticSim. stands for Semantic Similarity. For each column in each benchmark section, **bold** represents the best performance and underline stands for the second best one.

ral coherency. In the end, to evaluate the *generated hand quality*, we report Hand Structure Error (HS-Err) which is defined as in Eq. (2). We report all metrics on L frames in the videos not including the context image I .

Implementation Details For each video, we evenly sample 16 frames where the first frame is the context image I and the remaining 15 frames (i.e., $L = 15$) comprise the video to be denoised during training. The VAE [71], instruction tuning module [71], text encoder [71] and hand joints detection model [58] are previous work and frozen. The noise predictors are initialized with pretrained weights [25] and optimized during training. The coefficients in the loss functions are $\alpha = 0.1$ and $\eta = 0.1$. We train our model for 50 epochs with batch size 48 and learning rate 5×10^{-5} . These hyperparameters are chosen empirically on small subsets of the training data. We use mixed precision with bf16 on $6 \times$ H100 GPUs.

3.1. Comparisons with the State-of-the-Art

Baselines Our baseline methods include T12V models AnimateAnything [25], PIA [109], DynamiCrafter [93], AVDC [104] and LFDM [65], as well as T2V models CogVideoX (5B) [103], and Open Sora [111]. For space, we describe only some of these here. PIA integrates temporal alignment and conditioning layers but does not explicitly target hand precision in cluttered environments. DynamiCrafter adapts a video diffusion prior for animating still images by injecting text-aligned context representa-

tions. However, its reliance on implicit motion priors makes it susceptible to generating unnatural and extended dynamics when fine-grained hand-object interactions are required. For the T2V models, CogVideoX and Open Sora focus on generating long-form, high-motion videos but lack direct image conditioning, making them ineffective for HCVG as our results show. CogVideoX employs a 3D Variational Autoencoder and an expert transformer to improve temporal consistency but suffers from flickering artifacts across frames. Since none of the baselines are originally tailored for HCVG, we fine-tune all models on the Epic-Kitchens and Ego4D benchmarks for 50 epochs (200,000 iterations, batch size 16) for fair evaluation.

Quantitative and Qualitative Results Table 2 details our compelling quantitative comparisons. HANDI performs best across nearly *all* metrics and SOTA baselines, including the motion intensive samples—the subset of EK that have top 10% largest M_{video} (§2.1). In a few cases (4 values among 24), strong baselines (AVDC and AA) perform best; yet, neither shows consistent advantage across *any* metrics on all benchmarks. For example, although AVDC achieves the lowest FVD in EpicKitchens (the full set and motion-intensive subsets), it ranks the third for FVD on Ego4D, which is a more challenging benchmark with more diverse actions, objects, and environments (i.e., outside of the kitchen [32]). Notably, HANDI also produces the most semantically relevant videos, reflected in the highest CLIP_{Tx.} and BLIP scores, which measure alignment

Scope	No.	Mask	HRL	HS-Err. ↓	VisualSim.-Frame		VisualSim.-Video		Consistency	SemanticSim.	
					FID ↓	CLIP _{GT} ↑	FVD ↓	EgoVLP ↑	CLIP _{Cs.} ↑	CLIP _{Tx.} ↑	BLIP ↑
MA	1	×	×	0.02067	13.516	0.9551	172.56	0.211	0.9677	27.862	0.261
	2	Stage 1	×	0.01949	13.023	0.9549	122.31	0.214	0.9650	26.840	0.271
	3	×	✓	0.01771	13.440	0.9549	169.99	0.339	<u>0.9780</u>	27.863	0.269
	4	Stage 1	✓	0.01504	<u>10.692</u>	0.9563	100.52	0.390	0.9753	<u>28.041</u>	0.283
	5	Prior	✓	<u>0.01701</u>	12.530	0.9551	132.19	0.355	0.9848	27.909	0.275
	6	Prior	×	0.02149	11.335	0.9539	116.09	0.352	0.9714	28.011	0.262
	7	GT	×	0.01804	10.847	0.9547	<u>101.53</u>	0.367	0.9755	28.023	0.272
	8	GT	✓	0.01762	9.816	0.9536	114.44	<u>0.372</u>	0.9631	28.102	<u>0.281</u>
Full	1	×	×	0.01908	5.497	0.9588	171.29	0.338	0.9843	29.970	0.295
	2	Stage 1	×	0.01940	5.570	<u>0.9589</u>	124.42	0.197	0.9881	29.949	0.296
	3	×	✓	0.01760	5.384	<u>0.9589</u>	168.85	0.338	0.9889	29.929	0.294
	4	Stage 1	✓	0.01512	<u>5.272</u>	0.9590	101.89	0.377	0.9896	<u>30.055</u>	0.298
	5	Prior	✓	0.01670	5.285	0.9588	137.01	0.354	<u>0.9869</u>	30.045	<u>0.297</u>
	6	Prior	×	0.02146	5.613	0.9589	161.48	0.341	0.9748	30.025	0.296
	7	GT	×	0.01935	5.287	<u>0.9589</u>	<u>102.43</u>	<u>0.380</u>	0.9842	30.050	<u>0.297</u>
	8	GT	✓	0.01738	5.194	0.9587	113.57	0.382	0.9748	30.096	0.295

Table 3. Ablation study on the EpicKitchens benchmark [26], examining the impact of Motion Area (MA) mask generation (“Mask”) and Hand Refinement Loss (“HRL”) on model performance. The highlighted row is our full HANDI method. When Mask is “GT”, we use the ground truth mask which is supposed to be the upper bound of the performance but we still outperform it in more than half of the metrics.

with the text prompt. We discuss the (strong performance in the) hand structure error below in §3.2.

We show qualitative samples in Fig. 4 (and videos in supplementary materials). The key limitations of prior T2V methods are evident, including those performing well quantitatively (PIA, AVDC, AA). Despite their image-conditioning capabilities, these baselines suffer from unwanted background artifacts or blurry/rippled scene effects due to the lack of focus on the Motion Area. For example, AVDC generates blurry videos because it is designed for robot policy learning with low-resolution video. On the other hand, the hand quality generated baselines are rough or the motion is unnatural even if not affected by the scene effects (e.g. PIA and AA). These shortcomings stem from their lack of explicit hand-motion constraints, leading to minor flickering or unnatural hand movements. Likewise, the T2V baselines (Open Sora and CogVideoX) struggle in the HCVG setting, as expected with no image context.

Fig. 4 also shows how HANDI successfully localizes motion to the hand interaction region, avoiding unnecessary background changes and global effects. Motion flow analysis further corroborates this observation, showing that HANDI concentrates motion within the targeted region while competing methods exhibit undesired movement in surrounding areas.

Computational Efficiency Analysis Given HANDI’s two-stage design, one consideration is computational efficiency. Despite introducing an additional stage for motion area generation, our method remains highly efficient as it allows us to use a lightweight model structure for both stages to handle the easier MA task. We compare infer-

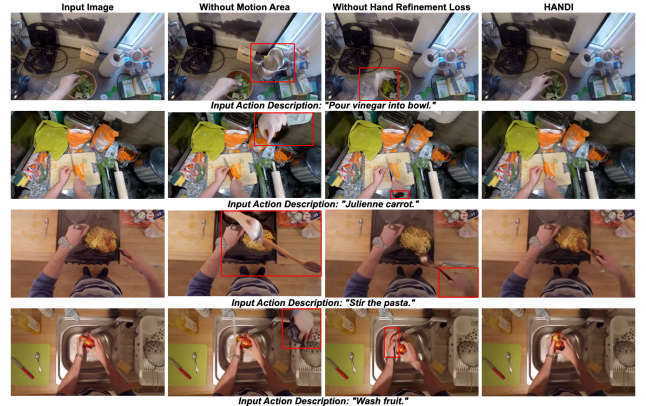


Figure 5. The visualization for ablation study showing the independent effectiveness of Motion Area generation and Hand Refinement Loss. The red boxes are not in the generated videos. They are drawn for better illustration, showing the area that reflects the effectiveness of the ablated components.

ence times for generating one video across the latest baselines: DynamiCrafter requires 9.32 seconds, CogVideoX takes 108.41 seconds, while HANDI completes generation in just 8.64 seconds, demonstrating that HANDI not only achieves superior video quality but also operates efficiently.

3.2. Ablation Study

We conduct an ablation study to investigate the effect of our two new model elements—generated Motion Area (MA) and Hand Refinement Loss (HRL); shown in Tab. 3 and Fig. 5. In the ablation, we not only assess performance on the full frames (Scope is “Full”) but also assess it on the

ground truth motion area M_{video} (§2.1) since this is the detailed hand-centric part of the video we focus on in HCGV (Scope is “MA”). Note that no mask (Mask is \times) means the motion area is set to the full frame for stage 2 generation.

Comparing rows 1 and 3 in both scopes assesses the impact of the model generated motion area. Clearly, allowing the system to generate a motion area in which to focus the stage 2 diffusion leads to higher quality video while preventing the generation of distractions and hallucinations in the background (as shown in Fig. 5). Rows 2 and 3 compare the impact of the HRL. As shown in Fig. 5 (rightmost two columns), without HRL, the generated hand could be blurry (fig. row 1 and 3) or cut off (fig. row 2) or distorted (fig. row 4). This demonstrates the capability of the HRL for detailed hand appearance improvement. Both sets of quantitative comparisons show significant improvements when the scope is set to the motion area, indicating better quality of the generated hand details, especially for FID and FVD, which capture the perceptual quality of the generated video.

4. Conclusion

We tackle the unique challenges in generating videos of hands performing goal oriented actions, an understudied aspect of video generation that is important for numerous applications, such as human and robot learning. In these hand-centric video generation tasks, one seeks high-fidelity hand structure with a stable video background based on the provided image and text conditioning. Our method, called HANDI, builds on the state of the art diffusion-based video generation literature with two important innovations. First, we automatically generate the motion area based on the visual context and the action prompt, allowing HANDI to focus on the region in the scene that is most relevant to the conditioning. Second, we propose a key hand refinement loss term that drives the diffusion model to focus on learning to generate high quality, realistic hand poses. Our SOTA comparisons and baselines on challenging real-world video datasets uniformly and significantly show the power of these two innovations. We have identified new avenues of future work for video generation in realistic hand-centric settings; for example, we plan to consider explicit models of the objects and tools in use for future work.

Acknowledgement

We would like to thank the anonymous reviewers for their valuable comments and suggestions. This work is sponsored by Defense Advanced Research Projects Agency (DARPA) HR00112220003 (Perceptually-enabled Task Guidance). The contents do not reflect the position of the U.S. Government.

References

- [1] Niki Aifanti, Christos Papachristou, and Anastasios Delopoulos. The mug facial expression database. In *11th International Workshop on Image Analysis for Multimedia Interactive Services WIAMIS 10*, pages 1–4, 2010. 16
- [2] Niki Aifanti, Christos Papachristou, and Anastasios Delopoulos. The mug facial expression database. In *11th International Workshop on Image Analysis for Multimedia Interactive Services WIAMIS 10*, pages 1–4. IEEE, 2010. 6
- [3] Kumar Ashutosh, Santhosh Kumar Ramakrishnan, Triantafyllos Afouras, and Kristen Grauman. Video-mined task graphs for keystone recognition in instructional videos. *Advances in Neural Information Processing Systems*, 36, 2024. 1
- [4] Kumar Ashutosh, Zihui Xue, Tushar Nagarajan, and Kristen Grauman. Detours for navigating instructional videos. In *Proceedings of the IEEE/CVF Conference on Computer Vision and Pattern Recognition*, pages 18804–18815, 2024. 1
- [5] Shikhar Bahl, Russell Mendonca, Lili Chen, Unnat Jain, and Deepak Pathak. Affordances from human videos as a versatile representation for robotics. 2023. 1
- [6] Max Bain, Arsha Nagrani, Gül Varol, and Andrew Zisserman. Frozen in time: A joint video and image encoder for end-to-end retrieval. In *IEEE International Conference on Computer Vision*, 2021. 16
- [7] Max Bain, Arsha Nagrani, Gül Varol, and Andrew Zisserman. Frozen in time: A joint video and image encoder for end-to-end retrieval. In *Proceedings of the IEEE/CVF international conference on computer vision*, pages 1728–1738, 2021. 6
- [8] Eslam Mohamed Bakr, Pengzhan Sun, Xiaojian Shen, Faizan Farooq Khan, Li Erran Li, and Mohamed Elhoseiny. Hrs-bench: Holistic, reliable and scalable benchmark for text-to-image models. In *Proceedings of the IEEE/CVF International Conference on Computer Vision*, pages 20041–20053, 2023. 6
- [9] Yuwei Bao, Keunwoo Yu, Yichi Zhang, Shane Storcks, Itamar Bar-Yossef, Alex de la Iglesia, Megan Su, Xiao Zheng, and Joyce Chai. Can foundation models watch, talk and guide you step by step to make a cake? In *Findings of the Association for Computational Linguistics: EMNLP 2023*, pages 12325–12341, 2023. 1
- [10] Samyadeep Basu, Mehrdad Saberi, Shweta Bhardwaj, Atoosa Malemir Chegini, Daniela Massiceti, Maziar Sanjabi, Shell Xu Hu, and Soheil Feizi. Editval: Benchmarking diffusion based text-guided image editing methods. *arXiv preprint arXiv:2310.02426*, 2023. 6
- [11] Filippos Bellos, Yayuan Li, Wuo Liu, and Jason Corso. Can large language models reason about goal-oriented tasks? In *Proceedings of the First edition of the Workshop on the Scaling Behavior of Large Language Models (SCALE-LLM 2024)*, pages 24–34, St. Julian’s, Malta, 2024. Association for Computational Linguistics. 1
- [12] T. Brooks, A. Holynski, and A. A. Efros. Instructpix2pix: Learning to follow image editing instructions. In *Proceed-*

- ings of *IEEE/CVF Conference on Computer Vision and Pattern Recognition*, 2023. 2
- [13] Zekun Cao and Regis Kopper. Real-time viewport-aware optical flow estimation in 360-degree videos for visually-induced motion sickness mitigation. In *Proceedings of the 25th Symposium on Virtual and Augmented Reality*, pages 210–218, 2023. 2
- [14] Zhi Cen, Huaijin Pi, Sida Peng, Zehong Shen, Minghui Yang, Zhu Shuai, Hujun Bao, and Xiaowei Zhou. Generating human motion in 3d scenes from text descriptions. In *CVPR*, 2024. 3
- [15] D. Ceylan, C.-H. P. Huang, and N. J. Mitra. Pix2video: Video editing using image diffusion. In *Proceedings of the IEEE/CVF International Conference on Computer Vision (ICCV)*, 2023. 2
- [16] Paul Chandler and John Sweller. Cognitive load theory and the format of instruction. *Cognition and instruction*, 8(4): 293–332, 1991. 1
- [17] Elliot Chane-Sane, Cordelia Schmid, and Ivan Laptev. Learning video-conditioned policies for unseen manipulation tasks. In *ICRA*, 2023. 1
- [18] S. Cheikh Youssef, A. Aydin, A. Canning, N. Khan, K. Ahmen, and P. Dasgupta. Learning surgical skills through video-based education: A systematic review. *Surgical Innovation*, 30(2):220–238, 2022. 1
- [19] C. Chen, R. Jafari, and N. Kehtarnavaz. UTD-MHAD: A Multimodal Dataset for Human Action Recognition Utilizing a Depth Camera and a Wearable Inertial Sensor. In *Proceedings of IEEE International Conference on Image Processing (ICIP)*, Canada, 2015. 16
- [20] Haoxin Chen, Menghan Xia, Yingqing He, Yong Zhang, Xiaodong Cun, Shaoshu Yang, Jinbo Xing, Yaofang Liu, Qifeng Chen, Xintao Wang, Chao Weng, and Ying Shan. Videocrafter1: Open diffusion models for high-quality video generation, 2023. 3
- [21] Haoxin Chen, Yong Zhang, Xiaodong Cun, Menghan Xia, Xintao Wang, Chao Weng, and Ying Shan. Videocrafter2: Overcoming data limitations for high-quality video diffusion models, 2024. 3
- [22] Tsai-Shien Chen, Aliaksandr Siarohin, Willi Menapace, Ekaterina Deyneka, Hsiang-wei Chao, Byung Eun Jeon, Yuwei Fang, Hsin-Ying Lee, Jian Ren, Ming-Hsuan Yang, et al. Panda-70m: Captioning 70m videos with multiple cross-modality teachers. In *Proceedings of the IEEE/CVF Conference on Computer Vision and Pattern Recognition*, pages 13320–13331, 2024. 6
- [23] Christian Dornhege Wolfram Burgard Christian Zimmermann Tim Welschehold and Thomas Brox. 3d human pose estimation in rgb-d images for robotic task learning. In *IEEE International Conference on Robotics and Automation (ICRA)*, 2018. 1
- [24] F. E. I. Craik. Effects of distraction on memory and cognition: a commentary. *Frontiers in Psychology*, 5(841):1–5. 1
- [25] Zuozhuo Dai, Zhenghao Zhang, Yao Yao, Bingxue Qiu, Siyu Zhu, Long Qin, and Weizhi Wang. Fine-grained open domain image animation with motion guidance. *arXiv preprint arXiv:2311.12886*, 2023. 2, 3, 4, 6, 7, 15, 16
- [26] Dima Damen, Hazel Doughty, Giovanni Maria Farinella, Antonino Furnari, Evangelos Kazakos, Jian Ma, Davide Moltisanti, Jonathan Munro, Toby Perrett, Will Price, et al. Rescaling egocentric vision: Collection, pipeline and challenges for epic-kitchens-100. *International Journal of Computer Vision*, pages 1–23, 2022. 1, 3, 5, 6, 7, 8, 15
- [27] Yilun Du, Sherry Yang, Bo Dai, Hanjun Dai, Ofir Nachum, Josh Tenenbaum, Dale Schuurmans, and Pieter Abbeel. Learning universal policies via text-guided video generation. *Advances in Neural Information Processing Systems*, 36, 2024. 2
- [28] Patrick Esser, Johnathan Chiu, Parmida Atighehchian, Jonathan Granskog, and Anastasis Germanidis. Structure and content-guided video synthesis with diffusion models. In *Proceedings of the IEEE/CVF International Conference on Computer Vision*, pages 7346–7356, 2023. 3
- [29] Qifan Fu, Xu Chen, Muhammad Asad, Shanxin Yuan, Changjae Oh, and Gregory Slabaugh. Handrawer: Leveraging spatial information to render realistic hands using a conditional diffusion model in single stage, 2025. 5
- [30] Nathan Gavenski, Odinaldo Rodrigues, and Michael Luck. Imitation learning: A survey of learning methods, environments and metrics. *arXiv e-prints*, pages arXiv–2404, 2024. 1
- [31] Michal Geyer, Omer Bar-Tal, Shai Bagon, and Tali Dekel. Tokenflow: Consistent diffusion features for consistent video editing, 2024. 2
- [32] Kristen Grauman, Andrew Westbury, Eugene Byrne, Zachary Chavis, Antonino Furnari, Rohit Girdhar, Jackson Hamburger, Hao Jiang, Miao Liu, Xingyu Liu, et al. Ego4d: Around the world in 3,000 hours of egocentric video. In *Proceedings of the IEEE/CVF Conference on Computer Vision and Pattern Recognition*, pages 18995–19012, 2022. 1, 3, 5, 6, 7, 15
- [33] Kristen Grauman, Andrew Westbury, Lorenzo Torresani, Kris Kitani, Jitendra Malik, Triantafyllos Afouras, Kumar Ashutosh, Vijay Baiyya, Siddhant Bansal, Bikram Boote, et al. Ego-exo4d: Understanding skilled human activity from first-and third-person perspectives. In *Proceedings of the IEEE/CVF Conference on Computer Vision and Pattern Recognition*, pages 19383–19400, 2024. 1
- [34] Yuwei Guo, Ceyuan Yang, Anyi Rao, Zhengyang Liang, Yaohui Wang, Yu Qiao, Maneesh Agrawala, Dahua Lin, and Bo Dai. Animatediff: Animate your personalized text-to-image diffusion models without specific tuning. *arXiv preprint arXiv:2307.04725*, 2023. 16
- [35] A. Haque, M. Tancik, A. A. Efros, A. Holynski, and A. Kanazawa. Instruct-nerf2nerf: Editing 3d scenes with instructions. In *Proceedings of the IEEE/CVF International Conference on Computer Vision (ICCV)*, 2023. 2
- [36] Kaiming He, Xiangyu Zhang, Shaoqing Ren, and Jian Sun. Deep residual learning for image recognition. In *Proceedings of the IEEE conference on computer vision and pattern recognition*, pages 770–778, 2016. 16
- [37] Martin Heusel, Hubert Ramsauer, Thomas Unterthiner, Bernhard Nessler, and Sepp Hochreiter. Gans trained by a two time-scale update rule converge to a local nash equilib-

- rium. *Advances in neural information processing systems*, 30, 2017. 6
- [38] Jonathan Ho, Ajay Jain, and Pieter Abbeel. Denoising diffusion probabilistic models. *Advances in neural information processing systems*, 33:6840–6851, 2020. 3
- [39] Jonathan Ho, Tim Salimans, Alexey Gritsenko, William Chan, Mohammad Norouzi, and David J Fleet. Video diffusion models. *Advances in Neural Information Processing Systems*, 35:8633–8646, 2022. 3
- [40] W. Hong, M. Ding, W. Zheng, X. Liu, and J. Tang. Cogvideo: Large-scale pretraining for text-to-video generation via transformers. In *Proceedings of the International Conference on Learning Representations*, 2023. 2
- [41] Kaiyi Huang, Kaiyue Sun, Enze Xie, Zhenguo Li, and Xihui Liu. T2i-compbench: A comprehensive benchmark for open-world compositional text-to-image generation. *Advances in Neural Information Processing Systems*, 36:78723–78747, 2023. 6
- [42] Vidhi Jain, Maria Attarian, Nikhil J Joshi, Ayzaan Wahid, Danny Driess, Quan Vuong, Pannag R Sanketi, Pierre Sermanet, Stefan Welker, Christine Chan, Igor Gilitschenski, Yonatan Bisk, and Debidatta Dwibedi. Vid2robot: End-to-end video-conditioned policy learning with cross-attention transformers, 2024. 1
- [43] Hanwen Jiang, Santhosh Kumar Ramakrishnan, and Kristen Grauman. Single-stage visual query localization in egocentric videos. *Advances in Neural Information Processing Systems*, 36, 2024. 1
- [44] Hak Gu Kim, Wissam J Baddar, Heoun-taek Lim, Hyunwook Jeong, and Yong Man Ro. Measurement of exceptional motion in vr video contents for vr sickness assessment using deep convolutional autoencoder. In *Proceedings of the 23rd ACM symposium on virtual reality software and technology*, pages 1–7, 2017. 2
- [45] Po-Chen Ko, Jiayuan Mao, Yilun Du, Shao-Hua Sun, and Joshua B Tenenbaum. Learning to act from actionless videos through dense correspondences. In *The Twelfth International Conference on Learning Representations*. 1
- [46] Po-Chen Ko, Jiayuan Mao, Yilun Du, Shao-Hua Sun, and Joshua B Tenenbaum. Learning to Act from Actionless Videos through Dense Correspondences. *arXiv:2310.08576*, 2023. 16
- [47] Bolin Lai, Xiaoliang Dai, Lawrence Chen, Guan Pang, James M Rehg, and Miao Liu. Lego: Learning egocentric action frame generation via visual instruction tuning. *arXiv preprint arXiv:2312.03849*, 2023. 1, 3, 6, 14
- [48] Colin Lea, Michael D Flynn, Rene Vidal, Austin Reiter, and Gregory D Hager. Temporal convolutional networks for action segmentation and detection. In *proceedings of the IEEE Conference on Computer Vision and Pattern Recognition*, pages 156–165, 2017. 4
- [49] Yann LeCun, Léon Bottou, Yoshua Bengio, and Patrick Haffner. Gradient-based learning applied to document recognition. *Proceedings of the IEEE*, 86(11):2278–2324, 1998. 4
- [50] Tony Lee, Michihiro Yasunaga, Chenlin Meng, Yifan Mai, Joon Sung Park, Agrim Gupta, Yunzhi Zhang, Deepak Narayanan, Hannah Teufel, Marco Bellagente, et al. Holistic evaluation of text-to-image models. *Advances in Neural Information Processing Systems*, 36, 2024. 6
- [51] Junnan Li, Dongxu Li, Caiming Xiong, and Steven Hoi. Blip: Bootstrapping language-image pre-training for unified vision-language understanding and generation. In *International conference on machine learning*, pages 12888–12900. PMLR, 2022. 6, 14
- [52] Zhengqi Li, Richard Tucker, Noah Snavely, and Aleksander Holynski. Generative image dynamics. In *Proceedings of the IEEE/CVF Conference on Computer Vision and Pattern Recognition*, pages 24142–24153, 2024. 2
- [53] B. Lin, Y. Ge, X. Cheng, Z. Li, B. Zhu, S. Wang, X. He, Y. Ye, S. Yuan, L. Chen, T. Jia, J. Zhang, Z. Tang, Y. Pang, B. She, C. Yan, Z. Hu, X. Dong, L. Chen, Z. Pan, X. Zhou, S. Dong, Y. Tian, and L. Yuan. Open-sora plan: Open-source large video generation model, 2024. 2
- [54] Kevin Qinghong Lin, Jinpeng Wang, Mattia Soldan, Michael Wray, Rui Yan, Eric Z Xu, Difei Gao, Rong-Cheng Tu, Wenzhe Zhao, Weijie Kong, et al. Egocentric video-language pretraining. *Advances in Neural Information Processing Systems*, 35:7575–7586, 2022. 6
- [55] Cheng Lu, Yuhao Zhou, Fan Bao, Jianfei Chen, Chongxuan Li, and Jun Zhu. Dpm-solver: A fast ode solver for diffusion probabilistic model sampling in around 10 steps. *Advances in Neural Information Processing Systems*, 35: 5775–5787, 2022. 3, 4
- [56] Cheng Lu, Yuhao Zhou, Fan Bao, Jianfei Chen, Chongxuan Li, and Jun Zhu. Dpm-solver++: Fast solver for guided sampling of diffusion probabilistic models. *arXiv preprint arXiv:2211.01095*, 2022. 3, 4
- [57] Wenquan Lu, Yufei Xu, Jing Zhang, Chaoyue Wang, and Dacheng Tao. Handrefiner: Refining malformed hands in generated images by diffusion-based conditional inpainting. In *ACM Multimedia 2024*, 2024. 3, 5
- [58] Camillo Lugaresi, Jiuqiang Tang, Hadon Nash, Chris McClanahan, Esha Uboweja, Michael Hays, Fan Zhang, Chuo-Ling Chang, Ming Guang Yong, Juhyun Lee, et al. Mediapipe: A framework for building perception pipelines. *arXiv preprint arXiv:1906.08172*, 2019. 4, 5, 7
- [59] X. Ma, Y. Wang, G. Jia, X. Chen, Z. Liu, Y.-F. Li, C. Chen, and Y. Qiao. Latte: Latent diffusion transformer for video generation, 2024. 2
- [60] Priyanka Mandikal and Kristen Grauman. Dexvip: Learning dexterous grasping with human hand pose priors from video. In *Conference on Robot Learning*, 2021. 1
- [61] Javier Marin, Aritro Biswas, Ferda Ofli, Nicholas Hynes, Amaia Salvador, Yusuf Aytar, Ingmar Weber, and Antonio Torralba. Recipe1m+: a dataset for learning cross-modal embeddings for cooking recipes and food images. *arXiv preprint arXiv:1810.06553*, 2018. 1, 3
- [62] Antoine Miech, Dimitri Zhukov, Jean-Baptiste Alayrac, Makarand Tapaswi, Ivan Laptev, and Josef Sivic. Howto100m: Learning a text-video embedding by watching hundred million narrated video clips. In *Proceedings of the IEEE/CVF international conference on computer vision*, pages 2630–2640, 2019. 1, 3

- [63] Suraj Nair, Aravind Rajeswaran, Vikash Kumar, Chelsea Finn, and Abhinav Gupta. R3m: A universal visual representation for robot manipulation. *arXiv preprint arXiv:2203.12601*, 2022. 16
- [64] Supreeth Narasimhaswamy, Uttaran Bhattacharya, Xiang Chen, Ishita Dasgupta, Saayan Mitra, and Minh Hoai. Handdiffuser: Text-to-image generation with realistic hand appearances. In *Proceedings of the IEEE/CVF Conference on Computer Vision and Pattern Recognition*, pages 2468–2479, 2024. 3, 5
- [65] Haomiao Ni, Changhao Shi, Kai Li, Sharon X Huang, and Martin Renqiang Min. Conditional image-to-video generation with latent flow diffusion models. In *Proceedings of the IEEE/CVF Conference on Computer Vision and Pattern Recognition*, pages 18444–18455, 2023. 3, 6, 7, 15, 16
- [66] Haomiao Ni, Bernhard Egger, Suhas Lohit, Anoop Cherian, Ye Wang, Toshiaki Koike-Akino, Sharon X Huang, and Tim K Marks. T2v-zero: Zero-shot image conditioning for text-to-video diffusion models. In *Proceedings of the IEEE/CVF Conference on Computer Vision and Pattern Recognition*, pages 9015–9025, 2024. 2
- [67] Alexander Quinn Nichol and Prafulla Dhariwal. Improved denoising diffusion probabilistic models. In *International conference on machine learning*, pages 8162–8171. PMLR, 2021. 3
- [68] Qin. Dexmv: Imitation learning for dexterous manipulation from human videos, 2021. 1
- [69] Alec Radford, Jong Wook Kim, Chris Hallacy, Aditya Ramesh, Gabriel Goh, Sandhini Agarwal, Girish Sastry, Amanda Askell, Pamela Mishkin, Jack Clark, et al. Learning transferable visual models from natural language supervision. In *International conference on machine learning*, pages 8748–8763. PMLR, 2021. 3, 6
- [70] Francesco Ragusa, Antonino Furnari, Salvatore Livatino, and Giovanni Maria Farinella. The meccano dataset: Understanding human-object interactions from egocentric videos in an industrial-like domain. In *Proceedings of the IEEE/CVF Winter Conference on Applications of Computer Vision*, pages 1569–1578, 2021. 1, 3
- [71] Robin Rombach, Andreas Blattmann, Dominik Lorenz, Patrick Esser, and Björn Ommer. High-resolution image synthesis with latent diffusion models. In *Proceedings of the IEEE/CVF conference on computer vision and pattern recognition*, pages 10684–10695, 2022. 2, 3, 4, 7
- [72] Chitwan Saharia, William Chan, Saurabh Saxena, Lala Li, Jay Whang, Emily L Denton, Kamyar Ghasemipour, Raphael Gontijo Lopes, Burcu Karagol Ayan, Tim Salimans, et al. Photorealistic text-to-image diffusion models with deep language understanding. *Advances in neural information processing systems*, 35:36479–36494, 2022. 2, 6
- [73] Christoph Schuhmann, Richard Vencu, Romain Beaumont, Robert Kaczmarczyk, Clayton Mullis, Aarush Katta, Theo Coombes, Jenia Jitsev, and Aran Komatsuzaki. Laion-400m: Open dataset of clip-filtered 400 million image-text pairs. *arXiv preprint arXiv:2111.02114*, 2021. 6
- [74] Fadime Sener, Dibyadip Chatterjee, Daniel Shelepov, Kun He, Dipika Singhania, Robert Wang, and Angela Yao. Assembly101: A large-scale multi-view video dataset for understanding procedural activities. In *Proceedings of the IEEE/CVF Conference on Computer Vision and Pattern Recognition*, pages 21096–21106, 2022. 1, 3
- [75] Uriel Singer, Adam Polyak, Thomas Hayes, Xi Yin, Jie An, Songyang Zhang, Qiyuan Hu, Harry Yang, Oron Ashual, Oran Gafni, et al. Make-a-video: Text-to-video generation without text-video data. *arXiv preprint arXiv:2209.14792*, 2022. 3
- [76] Aaron Smith, Skye Toor, and Patrick Van Kessel. Many turn to youtube for children’s content, news, how-to lessons. *Pew Research Center*, 7, 2018. 1
- [77] Yale Song, David Demirdjian, and Randall Davis. Tracking body and hands for gesture recognition: Natops aircraft handling signals database. In *Proceedings of the 9th IEEE International Conference on Automatic Face and Gesture Recognition (FG 2011)*, Santa Barbara, CA, 2011. 16
- [78] Achint Soni, Sreyas Venkataraman, Abhramil Chandra, Sebastian Fischmeister, Percy Liang, Bo Dai, and Sherry Yang. Videoagent: Self-improving video generation. *arXiv preprint arXiv:2410.10076*, 2024. 2
- [79] Tomáš Souček, Dima Damen, Michael Wray, Ivan Laptev, and Josef Sivic. Genhowto: Learning to generate actions and state transformations from instructional videos. In *2024 IEEE/CVF Conference on Computer Vision and Pattern Recognition (CVPR)*, pages 6561–6571. IEEE, 2024. 1, 3
- [80] Shane Storks, Itamar Bar-Yossef, Yayuan Li, Zheyuan Zhang, Jason J Corso, and Joyce Chai. Explainable procedural mistake detection. *arXiv preprint arXiv:2412.11927*, 2024. 1
- [81] Shuhan Tan, Tushar Nagarajan, and Kristen Grauman. Egodistill: Egocentric head motion distillation for efficient video understanding. *Advances in Neural Information Processing Systems*, 36:33485–33498, 2023.
- [82] Hao Tang, Kevin J Liang, Kristen Grauman, Matt Feiszli, and Weiyao Wang. Egotracks: A long-term egocentric visual object tracking dataset. *Advances in Neural Information Processing Systems*, 36, 2024. 1
- [83] Thomas Unterthiner, Sjoerd van Steenkiste, Karol Kurach, Raphaël Marinier, Marcin Michalski, and Sylvain Gelly. Fvd: A new metric for video generation. In *ICLR Workshop on Deep Generative Models for Structured Data (DeepGen-Struct)*, 2019. 6
- [84] Gül Varol, Ivan Laptev, and Cordelia Schmid. Long-term temporal convolutions for action recognition. *IEEE transactions on pattern analysis and machine intelligence*, 40 (6):1510–1517, 2017. 4
- [85] A Vaswani. Attention is all you need. *Advances in Neural Information Processing Systems*, 2017. 4
- [86] Su Wang, Chitwan Saharia, Ceslee Montgomery, Jordi Pont-Tuset, Shai Noy, Stefano Pellegrini, Yasumasa Onoe, Sarah Laszlo, David J Fleet, Radu Soricut, et al. Imagen editor and editbench: Advancing and evaluating text-guided image inpainting. In *Proceedings of the IEEE/CVF conference on computer vision and pattern recognition*, pages 18359–18369, 2023. 6

- [87] Xin Wang, Taemin Kwon, Mahdi Rad, Bowen Pan, Ishani Chakraborty, Sean Andrist, Dan Bohus, Ashley Feniello, Bugra Tekin, Felipe Vieira Frujeri, and Neel Joshi. Marc Pollefeys. Holoassist: an egocentric human interaction dataset for interactive ai assistants in the real world supplementary material. 1, 3
- [88] Xuan Wang, SK Ong, and Andrew Yeh-Ching Nee. Multimodal augmented-reality assembly guidance based on bare-hand interface. *Advanced Engineering Informatics*, 30(3): 406–421, 2016. 1
- [89] Xin Wang, Taemin Kwon, Mahdi Rad, Bowen Pan, Ishani Chakraborty, Sean Andrist, Dan Bohus, Ashley Feniello, Bugra Tekin, Felipe Vieira Frujeri, et al. Holoassist: an egocentric human interaction dataset for interactive ai assistants in the real world. In *Proceedings of the IEEE/CVF International Conference on Computer Vision*, pages 20270–20281, 2023. 1
- [90] Xiang Wang, Hangjie Yuan, Shiwei Zhang, Dayou Chen, Jiuniu Wang, Yingya Zhang, Yujun Shen, Deli Zhao, and Jingren Zhou. Videocomposer: Compositional video synthesis with motion controllability. *Advances in Neural Information Processing Systems*, 36, 2024. 3, 4, 16
- [91] Yaohui Wang, Xinyuan Chen, Xin Ma, Shangchen Zhou, Ziqi Huang, Yi Wang, Ceyuan Yang, Yanan He, Jiashuo Yu, Peiqing Yang, et al. Lavie: High-quality video generation with cascaded latent diffusion models. *International Journal of Computer Vision*, pages 1–20, 2024. 2
- [92] Jay Zhangjie Wu, Guian Fang, Haoning Wu, Xintao Wang, Yixiao Ge, Xiaodong Cun, David Junhao Zhang, Jia-Wei Liu, Yuchao Gu, Rui Zhao, et al. Towards a better metric for text-to-video generation. *arXiv preprint arXiv:2401.07781*, 2024. 6
- [93] Jinbo Xing, Menghan Xia, Yong Zhang, Haoxin Chen, Xintao Wang, Tien-Tsin Wong, and Ying Shan. Dynamicrafter: Animating open-domain images with video diffusion priors. 2023. 6, 7, 15
- [94] Haofei Xu, Jing Zhang, Jianfei Cai, Hamid Rezaatofghi, and Dacheng Tao. Gmflow: Learning optical flow via global matching. In *Proceedings of the IEEE/CVF Conference on Computer Vision and Pattern Recognition*, pages 8121–8130, 2022. 16
- [95] Jiale Xu, Xintao Wang, Yan-Pei Cao, Weihao Cheng, Ying Shan, and Shenghua Gao. Instructp2p: Learning to edit 3d point clouds with text instructions, 2023. 2
- [96] Hongwei Xue, Tiankai Hang, Yanhong Zeng, Yuchong Sun, Bei Liu, Huan Yang, Jianlong Fu, and Baining Guo. Advancing high-resolution video-language representation with large-scale video transcriptions. In *Proceedings of the IEEE/CVF Conference on Computer Vision and Pattern Recognition*, pages 5036–5045, 2022. 6
- [97] Hongwei Xue, Tiankai Hang, Yanhong Zeng, Yuchong Sun, Bei Liu, Huan Yang, Jianlong Fu, and Baining Guo. Advancing high-resolution video-language representation with large-scale video transcriptions. In *International Conference on Computer Vision and Pattern Recognition (CVPR)*, 2022. 16
- [98] Zihui Xue, Kumar Ashutosh, and Kristen Grauman. Learning object state changes in videos: An open-world perspective. *arXiv preprint arXiv:2312.11782*, 2023. 1
- [99] Chenggang Yan, Yunbin Tu, Xingzheng Wang, Yongbing Zhang, Xinhong Hao, Yongdong Zhang, and Qionghai Dai. Stat: Spatial-temporal attention mechanism for video captioning. *IEEE transactions on multimedia*, 22(1):229–241, 2019. 4
- [100] Yashuai Yan, Esteve Valls Mascaro, and Dongheui Lee. Imitationnet: Unsupervised human-to-robot motion retargeting via shared latent space. In *2023 IEEE-RAS 22nd International Conference on Humanoid Robots (Humanoids)*, pages 1–8, 2023. 1
- [101] Mengjiao Yang, Yilun Du, Kamyar Ghasemipour, Jonathan Tompson, Dale Schuurmans, and Pieter Abbeel. Learning interactive real-world simulators. *arXiv preprint arXiv:2310.06114*, 2023. 1, 2
- [102] Yue Yang, Atith N Gandhi, and Greg Turk. Annotated hands for generative models. *arXiv preprint arXiv:2401.15075*, 2024. 3, 5
- [103] Zhuoyi Yang, Jiayan Teng, Wendi Zheng, Ming Ding, Shiyu Huang, Jiazheng Xu, Yuanming Yang, Wenyi Hong, Xiaohan Zhang, Guanyu Feng, et al. Cogvideox: Text-to-video diffusion models with an expert transformer. *arXiv preprint arXiv:2408.06072*, 2024. 6, 7, 15
- [104] Du Yilun, Yang Mengjiao, Dai Bo, Dai Hanjun, Nachum Ofir, Tenenbaum Joshua B, Dale Schuurmans, and Pieter Abbeel. Learning universal policies via text-guided video generation. *arXiv e-prints*, pages arXiv–2302, 2023. 6, 7, 15, 16
- [105] Shengming Yin, Chenfei Wu, Jian Liang, Jie Shi, Houqiang Li, Gong Ming, and Nan Duan. Dragnuwa: Fine-grained control in video generation by integrating text, image, and trajectory. *arXiv preprint arXiv:2308.08089*, 2023. 2, 3
- [106] H. Yuan, S. Zhang, X. Wang, Y. Wei, T. Feng, Y. Pan, Y. Zhang, Z. Liu, S. Albanie, and D. Ni. Instructvideo: Instructing video diffusion models with human feedback. In *Proceedings of the IEEE/CVF Conference on Computer Vision and Pattern Recognition (CVPR)*, pages 6463–6474, 2024. 2
- [107] D. J. Zhang, J. Z. Wu, J.-W. Liu, R. Zhao, L. Ran, Y. Gu, D. Gao, and M. Z. Shou. Show-1: Marrying pixel and latent diffusion models for text-to-video generation. *International Journal of Computer Vision*, 2024. 2
- [108] Mingyuan Zhang, Zhongang Cai, Liang Pan, Fangzhou Hong, Xinying Guo, Lei Yang, and Ziwei Liu. Motiandiffuse: Text-driven human motion generation with diffusion model. *arXiv preprint arXiv:2208.15001*, 2022. 3
- [109] Yiming Zhang, Zhening Xing, Yanhong Zeng, Youqing Fang, and Kai Chen. Pia: Your personalized image animator via plug-and-play modules in text-to-image models. In *Proceedings of the IEEE/CVF Conference on Computer Vision and Pattern Recognition*, pages 7747–7756, 2024. 2, 6, 7, 15
- [110] Boyuan Zheng, Sunny Verma, Jianlong Zhou, Ivor W Tsang, and Fang Chen. Imitation learning: Progress, taxonomies and challenges. *IEEE Transactions on Neural Networks and Learning Systems*, 2022. 1

- [111] Zangwei Zheng, Xiangyu Peng, Tianji Yang, Chenhui Shen, Shenggui Li, Hongxin Liu, Yukun Zhou, Tianyi Li, and Yang You. Open-sora: Democratizing efficient video production for all, 2024. [6](#), [7](#), [15](#)
- [112] Luowei Zhou, Chenliang Xu, and Jason Corso. Towards automatic learning of procedures from web instructional videos. In *Proceedings of the AAAI Conference on Artificial Intelligence*, 2018. [1](#), [3](#)

A. Ablation Study Qualitative Results Shown in Videos

For the best visualization of motion, we encourage readers to visit the videos for ablation study qualitative results, attached [ablation.mp4](#) or in project page.

B. More Qualitative Results Comparing with SOTA methods Shown in Videos

Likewise, for comparison with SOTA methods, we encourage readers to view 10 qualitative results in videos in the off-line HTML page attached [baseline_comparison/index1.html](#) or the online project page. A screenshot of the page is shown in Fig. 6 for readers’ reference.

By comparing with all baselines, we emphasize three key capabilities of our method that are accountable for the two key designs—Motion Area (MA) Generation and Hand Refinement Loss (HRL). Specifically, we observe good performance on generating Hand-Centric videos for actions require (i) intricate fingertip motion; (ii) large Motion Area; (iii) Object State Changing. Our proposed learnable automatic Motion Area mask generation helps the model to focus on the accurate region for the action execution (“ii” and “iii”), avoiding adding distraction to background. Our novel Hand Refinement Loss helps the model handle the actions with critical details (“i”), which is under-explored in previous work. In this gallery, for each sample, the first row displays the input context image and the results from different methods. In the second row, we first present the predicted Motion Area mask from our Stage 1 model. Then in the same row, we show the motion flow below generated video from each method. Note that the motion flow is not part of the model’s outputs; it is shown solely to facilitate easier comparison among methods. Below the visuals, we provide the input Text Prompt for the target action (e.g., “Pick up and crack egg.”) and the Enriched Action Description (e.g., “The person uses their left hand to pick up an egg from the egg box and cracks it into a bowl.”).

C. BLIP Score with Different BLIP Model Size

BLIP Score [47] leverage pre-trained BLIP model [51] to evaluate how close the generated video content is to the target action text description. In the main script, we introduce the evaluation results using the large BLIP model. In this supplementary material, we provide evaluation results from the small BLIP model as well. These results yield the same conclusion as we have in the main script — our method outperforms other baseline methods.

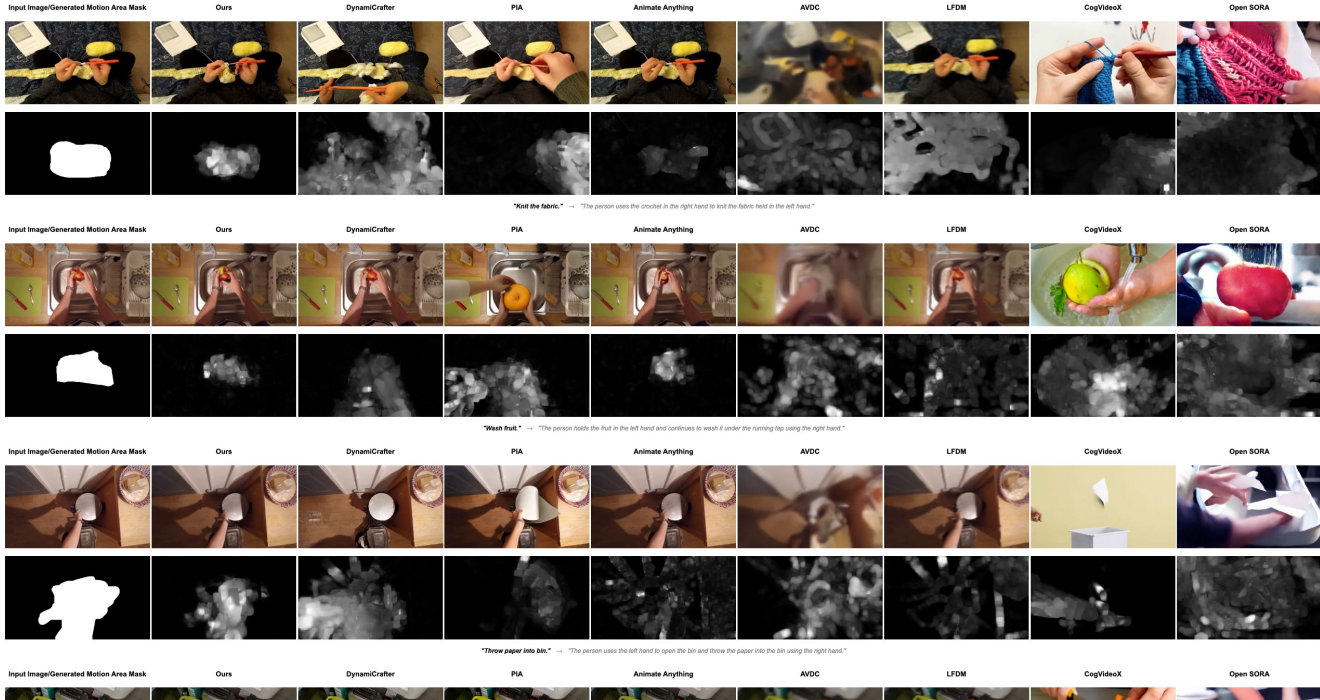


Figure 6. An overview of the HTML page that shows more qualitative results in videos. Please view the full page in attachment [baseline_comparison/index1.html](https://baseline-comparison/index1.html) or the online project page.

Dataset	Method	BLIP_large \uparrow	BLIP_base \uparrow
EpicKitchens	LFDM [65]	0.235	0.223
	AA [25]	0.295	0.298
	AVDC [104]	0.116	0.106
	PIA [109]	0.294	0.299
	HANDI	0.298	0.335
Ego4D	LFDM [65]	0.221	0.219
	AA [25]	0.260	0.264
	AVDC [104]	0.155	0.161
	PIA [109]	0.219	0.260
	HANDI	0.263	0.306

Table 4. Quantitative results on EpicKitchens [26], Ego4D [32] and a Motion Intensive subset of EpicKitchens. Our method outperforms all baselines across all metrics on at least one dataset.

D. Generation of Various Actions in the Same Visual Context

We explore our model’s performance on generating different actions given the same input context image. These are novel image-action pairs that have never shown in the dataset including the test set. We illustrate one example in Fig. 7 that crosses two existing samples in the test set. These results further indicate that our model can generate Hand-Centric videos for various actions, emphasizing hand

movement and subtle fingertip motion.

E. Motion Flow

As we shown in the qualitative results in both main paper and supplementary materials, we compute Motion Flow to assist the illustration of the motion in the generated video from each method. We first compute optical flow between all two consecutive frames in the generated video. Then we overlay all optical flows in a way that counting the number of frames that has optical flow intensity for each pixel. Therefore, the produced map has the same size as the optical flow (and the generated video) where each pixel has the intensity $m' \in [0, \dots, L]$ (inclusive) where L is the number of generated frames. In the end, we normalize the intensities by L to produce our visualized Motion Flow where each pixel has the intensity $m \in [0, 1]$ (inclusive).

F. Baseline Implementation Details

Since previous Text-Image-to-Video/Image Animation work does not report results on the Hand-Centric Video Generation (HCVG) task, we implement all four baselines. For a fair comparison, we train or fine-tune their methods on the same training set used for our own method. For DynamCrafter [93], CogVideoX [103], and Open Sora [111], we directly run the published codebase with fine-tuning and inference code to obtain our reported results. We provide

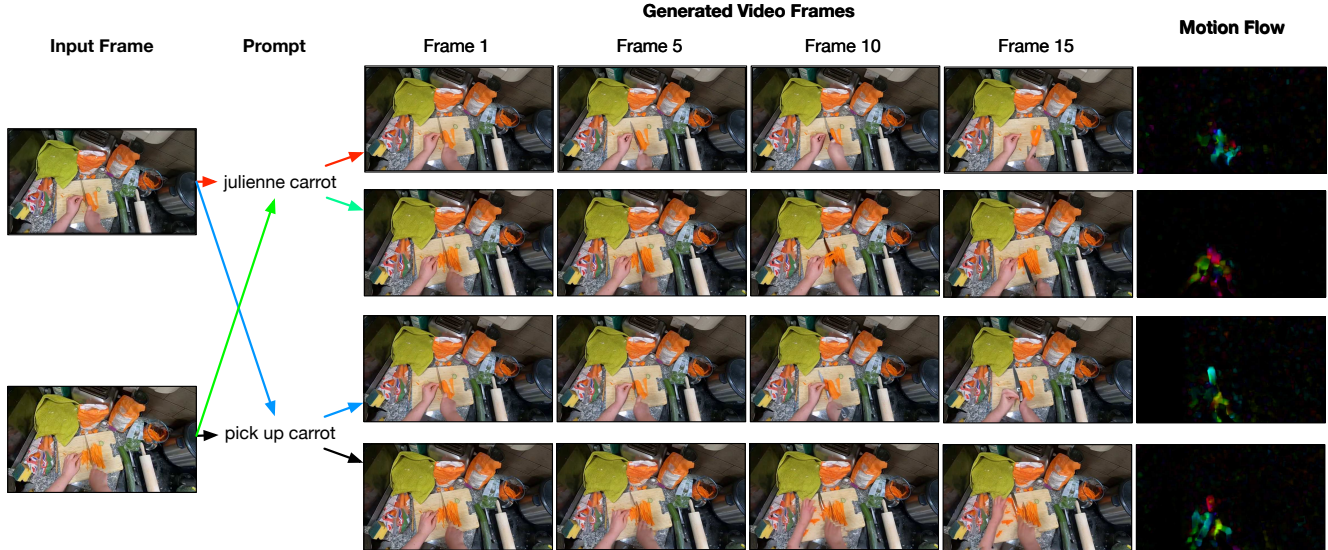


Figure 7. An illustration that crosses the input action text and context image in two test samples. Our method generates reasonable Hand-Centric videos for such challenging scenarios of subtle actions.

more details about the implementation as follows:

F.1. Animate Anything

The *Animate Anything* [25] model is initialized from VideoComposer [90], which is pre-trained on the WebVid10M [6] dataset, a large-scale video dataset designed for general video generation tasks. For fine-tuning, the model is trained on 20,000 videos randomly sampled from the HDVILA-100M dataset [97]. These samples are carefully selected to remove watermarks, ensuring higher-quality training data. The model leverages a latent diffusion framework to generate fine-grained animations guided by motion area masks and motion strength.

F.2. Latent Flow Diffusion Model (LFDM)

LFDM [65] is a versatile framework with multiple pre-trained versions. The available pre-training datasets include:

- **The MUG Facial Expression Dataset [1]:** Contains 1,009 videos of 52 subjects performing 7 different facial expressions.
- **The MHAD Human Action Dataset [19]:** Comprises 861 videos of 27 actions performed by 8 subjects.
- **The NATOPS Aircraft Handling Signal Dataset [77]:** Consists of 9,600 videos of 20 subjects performing 24 body-and-hand gestures used for communicating with U.S. Navy pilots.

For the experiments, the version pre-trained on the MHAD Human Action Dataset is used. LFDM generates 8-frame video sequences, employing a two-stage training process: an unsupervised latent flow auto-encoder and a condi-

tional 3D U-Net-based diffusion model for temporal latent flow generation. Training is computationally efficient, requiring only 4 GPUs for a single day of training.

F.3. Personalized Image Animator (PIA)

PIA is trained on the WebVid10M dataset [6], focusing only on the condition module and temporal alignment layers as trainable parameters. The motion module from AnimateDiff [34] is used as a pre-trained model for initializing the temporal alignment layers. PIA fine-tunes on curated images generated by personalized text-to-image (T2I) models, combined with motion-related prompts. These curated images and prompts are included in the AnimateBench benchmark, which consists of diverse images across multiple styles and tailored motion-related annotations. Fine-tuning focuses on the condition module and temporal alignment layers while freezing the base T2I model.

F.4. Actions from Video Dense Correspondences (AVDC)

AVDC [46, 104] is trained on a collection of video datasets featuring table-top manipulation and navigation tasks. Although the specific dataset names are not provided, the training framework synthesizes 8-frame video sequences using a text-conditioned video diffusion model. The weights of the ResNet-18 [36] backbone are initialized either from scratch (BC-Scratch) or using the pre-trained parameters of R3M [63]. GMFlow [94] is employed for optical flow prediction, enabling dense correspondences for action regression. The model training is computationally optimized to run on 4 GPUs within a single day.